Revision 1

Interlayer structure model of tri-hydrated low-charge smectite by X-ray diffraction and Monte Carlo modeling in the Grand Canonical ensemble.

Baptiste Dazas[1,2,*]

Eric Ferrage[3]

Alfred Delville[4]

Bruno Lanson[1,2]

(1) Univ. Grenoble Alpes, ISTerre, F-38041 Grenoble, France.
(2) CNRS, ISTerre, F-38041 Grenoble, France.
(3) Univ. Poitiers – CNRS, IC2MP−HydrASA, F-86022 Poitiers, France.
(4) Univ. Orléans – CNRS, Centre de Recherche sur la Matière Divisée, F-45071 Orléans, France

* Corresponding author. E-mail: baptiste.dazas@ujf-grenoble.fr

ABSTRACT

The present study aims primarily at refining a structure model for interlayer cations and H_2O molecules in tri-hydrated (3W) smectite (d_{001} = 18-19 Å). The < 2 µm fraction of the SWy-2 source clay (low-charge montmorillonite) was saturated by Mg^{2+}, Ca^{2+}, Ba^{2+} or Na^+ cations, before collection of X-ray diffraction (XRD) patterns at 98% relative humidity. Experimental d_{001} values derived for the essentially homogeneous 3W hydrates provided volume constraints for Grand Canonical Monte Carlo (GCMC) simulations. Computed atomic density distribution of interlayer species were used in turn to calculate XRD intensities of 00*l* reflections. The agreement between calculated and experimental 00*l* intensities allowed validating the GCMC results of both interlayer H_2O content and distribution of interlayer species (cations and H_2O molecules). Computed atomic density profiles do not correspond to the usual model of three discrete planes of H_2O molecules but rather exhibit two sharp planes of H_2O molecules wetting the clay surfaces (at ~2.7 Å from the clay layer surface). Additional H_2O molecules belong to cation hydration shells or define a poorly organized ensemble filling internal voids. This alternative model suggests that the stability of the 3W hydrate results from the dual interaction of some H_2O molecules with interlayer cation, through their second hydration shell, and with the 2:1 clay surface. Computed atomic density profiles were approximated to propose an interlayer structure model for 3W smectite. This simplified model includes two sets of two planes (symmetrical relative to the interlayer mid-plane) for H_2O molecules and one set for interlayer cations. This model allows reproducing experimental XRD patterns for the different samples investigated and thus represents a valid set of parameters for routine quantitative analysis of XRD profiles in an effort to determine smectite reactivity close to water saturated conditions. Implications of such studies are crucial to provide experimental constraints on the behavior of the main vector of element transfer under conditions common in surficial environments and prevailing in waste repositories. In addition, the present study provides an experimental validation of structure models derived from the widely used ClayFF model, and thus allows its use to predict the fate of water in clayey systems close to water saturated conditions.

Keywords: Crystal structure, smectite-water, tri-hydrated, water in smectite interlayer, montmorillonite, X-ray diffraction, Monte-Carlo, simulation.

INTRODUCTION

Smectite clays are ubiquitous in surface environments and sedimentary rocks, frequently as a major mineral component. Smectite layered structure is composed of two tetrahedral sheets sandwiching an octahedral sheet to form a TOT or 2:1 layer. Isomorphic substitutions by lower-valence cations occurring in tetrahedral and/or octahedral sheets induce a net negative charge of the TOT layer. This deficit is compensated for by the presence in the interlayer space of exchangeable cations whose hydration properties control smectite colloidal behavior and crystalline swelling (Mooney et al. 1952; Sato et al. 1992; Berend et al. 1995; Boek et al. 1995a; Cases et al. 1997; Young and Smith 2000; Marry and Turq 2003). The latter is characterized by the stepwise expansion of the layer-to-layer distance with increasing water activity. This expansion has been commonly described in the literature as the incorporation of 1, 2, and, less frequently, 3 planes of interlayer H_2O molecules, leading to the well-known 1W (d_{001} = 11.6-12.9 Å), 2W (d_{001} = 14.9-15.7 Å), and 3W (d_{001} = 18-19 Å) hydration states, in addition to the dehydrated one (0W, d_{001} = 9.6-10.2 Å – (Nagelschmidt 1936; Bradley et al. 1937; Hendricks and Merrill 1938; Mooney et al. 1952; Norrish 1954; Walker 1955). Smectite hydration plays a pivotal role in the physical and chemical behaviors of the environments where smectite is found (*e.g.*, Burst 1969; Bouma et al. 1977; Vrolijk 1990; Matsuda et al. 2004; Takahashi et al. 2005; Boutareaud et al. 2008; Boullier et al. 2009; Tertre et al. 2011a, 2011b; Bittelli et al. 2012). More specifically, smectite hydration degree can strongly impact dynamical properties of interlayer cations (Malikova et al. 2006, 2007, 2010; Marry et al. 2011; Michot et al. 2012) and thus the transfer and fate of H_2O and pollutants. For example, the prediction of radionuclide migration in clay-based engineered barriers is controlled essentially by smectite influence on solute transfers (Turner et al. 1996; Baeyens and Bradbury 1997; Suzuki et al. 2004;

Tournassat et al. 2004; Van Loon et al. 2004; Tertre et al. 2005, 2006; Glaus et al. 2007; Gates et al. 2009; Sánchez et al. 2009).

Smectite hydration and interlayer structure of 0W, 1W, and 2W hydrates have been extensively studied for decades both from experimental and computational perspectives, mainly using X-ray diffraction (XRD) and Monte Carlo simulations (Fu et al. 1990; Boek et al. 1995a, 1995b; Chang et al. 1995, 1997; Skipper et al. 1995; Karaborni et al. 1996; Moore and Reynolds 1997; Zeng et al. 2004; Meleshyn and Bunnenberg 2005; Smith et al. 2006; Sakharov and Lanson 2013 and references therein), respectively. These studies provided a comprehensive picture of interlayer H_2O and cation configurations in both 1W and 2W hydration states, leading to structure models commonly used for the calculation of XRD profiles. Such calculations have allowed investigating smectite reactivity under various conditions such as cation exchange, water activity, and temperature (*e.g.*, Ferrage et al. 2005a, 2007a; Oueslati et al. 2009; Dazas et al. 2013). No structure model is available for the 3W hydrate however, likely because of the scarcity of experimental studies devoted to this hydration state. The 3W smectite interlayer structure was thus approximated as a marginal contribution from XRD data (Pons et al. 1981a, 1981b; Cases et al. 1992, 1997; Berend et al. 1995; Kawamura et al. 1999; Holmboe et al. 2012; Dazas et al. 2013) or derived from theoretical simulations (Chang et al. 1995; Tambach et al. 2004; Tao et al. 2010) without quantitative comparison with independent data. Modeling of XRD data from 3W-smectite containing structures and mixtures thus remains highly imprecise despite the overwhelming presence of this hydration state under conditions close to water saturation, where most of the solute transfer processes occur (Melkior et al. 2005, 2007, 2009; Van Loon et al. 2005; Appelo et al. 2010).

In the present study, the interlayer structure of 3W montmorillonite was investigated for four interlayer cations (Mg^{2+}, Ca^{2+}, Ca^{2+} and Na^{+}). Within this scope, results from XRD profile modeling and Monte Carlo simulations performed in the Grand Canonical ensemble where thus collated, following a strategy similar to that used by Ferrage et al. (2011) for 1W and 2W saponites. Upon validation, molecular simulation results are used (i) to gain a comprehensive understanding of the parameters controlling the structure and stability of the 3W hydrate and (ii) to derive a simplified interlayer structure model allowing the routine calculation of XRD profiles.

MATERIALS AND METHODS

Samples

The SWy-2 reference montmorillonite from the Source Clay Repository (http://www.clays.org/SOURCE%20CLAYS/SCavailable.html) was used. This montmorillonite is originally Na-saturated, and exhibits a low octahedral charge and extremely limited tetrahedral substitutions with structural formula $[(Al_{3.00}Mg_{0.52}Fe_{0.43})(Si_{7.97}Al_{0.03})O_{20}(OH)_4]M^{+}_{0.70}$ (< 2 µm size fraction – Stucki et al. 1984; Mermut et al. 2001). The < 2 µm fraction was obtained by centrifugation and used to prepare 4 samples with a variety of interlayer cations. Ion exchange was performed at room temperature with 1 $mol.L^{-1}$ aqueous solutions of Mg-, Ca-, Ba-, and Na-chlorides. SWy-2 suspensions were shaken mechanically for 24 h in each saline solution (~50 mg of solid in ~50 mL solution) before separation of the solid fraction by centrifugation and addition of fresh saline solution. Saturation steps were repeated three times to ensure a complete cation exchange. Removal of the excess chloride was then performed by washing the solid three times by immersion for 24 h in deionized water (Siemens® UltraClear, 18.2 MΩ.cm^{-1}). Samples are hereafter referred to as Mg-, Ca-, Ba- and Na-SWy.

X-ray diffraction (XRD) and profile modeling of 00*l* reflections

Oriented slides were prepared for all four samples by drying at room temperature an aqueous clay suspension on a glass slide. XRD patterns were then recorded using a Bruker D8 equipped with a MHG Messtechnik humidity controller coupled to an Anton Paar CHC+ chamber. Intensities were measured with a SolXE Si(Li) solid-state detector from Baltic Scientific Instruments for 4 s per 0.04° 2θ step over the 2-50° 2θ CuKα range. The divergence slit, the two Soller slits, the antiscatter and resolution slits were 0.3°, 2.3°, 2.3°, 0.3°, and 0.1°, respectively. Samples were initially equilibrated at ~50% relative humidity (RH) in the chamber. The humidity was then increased steadily up to 98%RH (~5 hour ramps), where diffraction patterns were recorded. Each pattern was recorded twice to ensure the stability of the hydration state. The layer-to-layer distances were found to be 19.23 Å, 18.93 Å, 18.90 Å, and 18.73 Å for Mg-SWy, Ca-SWy, Ba-SWy, and Na-SWy, respectively (Table 1). The low values determined for the ξ parameter, calculated as the standard deviation of the $l \times d_{00l}$ values (in Å) for the ten 00*l* reflections measurable over the 2-50° 2θ range (Table 1), indicated a homogeneous 3W state (Ferrage et al. 2005b, 2007b). The algorithms developed initially by Drits and co-workers were used to fit XRD data over the recorded 2-50° 2θ range (Drits and Sakharov 1976; Drits and Tchoubar 1990). Instrumental and experimental factors such as horizontal and vertical beam divergences, goniometer radius, and length and thickness of the oriented slides were measured and introduced without further adjustment. The mass absorption coefficient (μ*) was set to 45 cm^{2}g^{-1}, as recommended by Moore and

Reynolds (1997). Additional variable parameters included the size of coherent scattering domains along the c* axis which was characterized by a maximum value, set to 80 layers, and by a mean value N equal to 7.5, 7.0, 7.5 and 5.7 layers for Mg-SWy, Ca-SWy, Ba-SWy and Na-SWy, respectively. Usual *z*-coordinates of atoms building the smectite TOT layer (Moore and Reynolds 1997) were used. Consistent with the rational series of d_{001} values, preliminary fits of XRD data revealed a proportion of 3W layers of 97-98% for Mg-SWy, Ca-SWy, and Ba-SWy and of 92% for Na-SWy (Table 1).

Grand Canonical Monte Carlo (GCMC) simulations

Monte Carlo simulations were performed in the Grand Canonical ensemble (Adams 1974, 1975; Allen and Tildesley 1994) to assess the content of interlayer H_2O and the equilibrium state of interlayer species (H_2O and cations) at 98% RH and 300 K, using a homemade program (Delville 1991; Rinnert et al. 2005; Michot et al. 2007, 2012; Porion et al. 2008; Ferrage et al. 2011; Jiménez-Ruiz et al. 2012). The rigid simulation box included 3 interlayers and related 2:1 layers (Figure 1). Each layer encompassed 6 and 4 unit cells along the *a* and *b* directions, respectively, with a –*a*/3 layer displacement leading to a face to face configuration for ditrigonal cavities. The layer-to-layer distance was consistent with experimental d_{001} values (Table 1). The ideal composition $[(Al_{3.25}Mg_{0.75})(Si_{8.00})O_{20}(OH)_4]M^{+}_{0.75}$ was used for 2:1 layers. Mg-for-Al substitutions were located randomly in each layer with an exclusion rule preventing two Mg atoms from occupying neighboring octahedra. The ClayFF force field (Cygan et al. 2004) and SPC (Berendsen et al. 1981) water model were selected to simulate the clay-water interactions. Lennard-Jones potentials of interlayer cations derived by Åqvist (1990) were used. For a given partial pressure, water chemical potential is given by the following relation:

$$\frac{\mu}{kT} = \frac{\mu^0}{kT} + \ln\left(\frac{P}{P^0}\right) \qquad \text{(Eq. 1)}$$

with

$$\frac{\mu^0}{kT} = \ln(\Lambda^3 \times \rho) \qquad \text{(Eq. 2)}$$

considering H_2O vapor as an ideal fluid, , Λ being H_2O de Broglie wavelength (0.238376 Å), *k* the Boltzmann constant and ρ H_2O vapor density at 300 K (7.7087481×10^{-7} molecules.$Å^{-3}$). GCMC simulations encompassed 6 000 blocks, each with 10 000 elementary steps allowing stabilization of interlayer H_2O molecules content. At each step one of the clay interlayers was selected randomly, and with an equal probability an attempt was made (i) to remove a H_2O molecule, (ii) to add a H_2O molecule in a random configuration, or (iii) to move a randomly chosen cation or H_2O molecule. During calculations, an Ewald summation (Heyes 1994) was used in addition to the three-dimensional minimum image convention to ensure the convergence of the electrostatic energy. A final run including 1 000 blocks of 5 000 steps was performed to generate the equilibrium properties of interlayer species and to derive radial cation-H_2O distribution functions and uncertainties on computed parameters (calculated as twice the standard deviation). Finally, interlayer atomic density profiles were subdivided in 40 slices parallel to the layer plane to calculate 00*l* XRD reflections.

RESULTS

GCMC simulations

Atomic density profiles derived from GCMC simulations are shown in Figure 2a, whereas Table 2 reports H_2O contents computed at equilibrium. The latter values are similar for all cations investigated and range from 14.82-16.02 H_2O molecules per formula unit (p.f.u. – Table 2). Similarly, atomic density profiles of oxygen and hydrogen display similar features for all samples (Figure 2a). Oxygen profiles systematically exhibit two discrete maxima at ~2.7 Å from the 2:1 layer surface with a full width at half maximum intensity (FWHM) of ~0.94 Å. An additional "plane" of H_2O molecules layer is centered on the interlayer mid-plane (Figure 2a). Contrasting with the previous set of two discrete maxima, this third "plane" is poorly resolved, indicative of an increased organizational disorder. Hydrogen profiles are weakly modulated except close to the 2:1 layer surface where two discrete and sharp maxima result from the polarization of H_2O molecules (Henderson 2002; Ferrage et al. 2011). Finally, cations are located mainly on the interlayer mid-plane (Mg- and Ca-SWy) with the presence of two distinct maxima for Ba- and Na-SWy owing to a slight positional shift towards the 2:1 layer (Figure 2a).

Simulation of 00*l* reflections with GCMC-computed atomic profiles

Although atomic density profiles are similar for all samples (Figure 2a), the sensitivity of XRD towards interlayer species depends on their electron content. GCMC-computed atomic density profiles can be converted to electronic density profiles (considering neutral atoms) to assess the actual contrast between different interlayer configurations. With 8 and 1 e^- for oxygen and hydrogen, respectively, the electronic density profiles of interlayer H_2O molecules resemble those of oxygen and do not differ strongly from one sample to the other (Figure 2b). On the contrary, the Z-contrast is enhanced for cations (Na: 11 e$^-$, Mg: 12 e$^-$, Ca: 20 e$^-$, and Ba: 56 e$^-$), with additional contrast induced by their contrasting valence. Both effects lead to distinct electronic density profiles as a function of interlayer cation (Figure 2b).

These electron density profiles may be used in turn to calculate 00*l* reflection intensity distributions (Figure 3a). The quality of the fit to the data validates the GCMC-computed atomic density profiles shown (Figure 2a) and allows using this computational technique to gain additional insights into the local configuration of interlayer cations and H_2O molecules in 3W montmorillonite.

DISCUSSION

Assessment of the methodology used to determine interlayer configuration in 3W montmorillonite

Validation of GCMC interlayer configuration. The approach used in the present study to determine the interlayer structure of 3W montmorillonite is similar to that developed by Ferrage et al. (2011) for 1W and 2W synthetic saponites, with the quantitative comparison of GCMC simulations and experimental results. Such quantitative cross-validation represents a step further for the validation of molecular simulations compared to the common qualitative comparison between computational and experimental results (*e.g.*, Kawamura et al. 1999; Greathouse and Storm 2002; Porion et al. 2003; Ferrage et al. 2005c; Heinz et al. 2005; Rinnert et al. 2005; Smith et al. 2006; Tambach et al. 2006). In the present work the number of experimental constraints is reduced compared to the original work of Ferrage et al. (2011) which included neutron and X-ray diffraction data as well as gravimetric measurement of water contents. The interlayer H_2O content of 3W montmorillonite cannot be compared directly to water sorption data owing to the presence of large contents of interparticular (pore) water which precludes the experimental determination of crystalline water at high RH values (Sing 1982; Michot et al. 1995; Ferrage et al. 2010). The validity of the present GCMC interlayer configurations was not assessed either through the comparison with neutron diffraction data on deuterated specimens (ND-D_2O) to benefit from the additional sensitivity to interlayer D_2O distribution due to the scattering length of the deuterium isotope. Ferrage et al. (2011) evidenced however a similar sensitivity of both XRD and ND-D_2O to the modeling of water-clay interactions. The good quality fits obtained in the present study (Figure 3a) thus indicate a realistic description of clay-water interactions in 3W montmorillonite when using the ClayFF force field and SPC water model. In addition, by using a set of different cations, the present study provides additional information on cation-clay and cation-water interactions. Although interlayer H_2O profiles are similar for all samples, the different scattering factors of cations induce contrasting contributions to XRD (Figure 2b), experimental variations of 00*l* reflection intensities being likely related to the cation contribution (Figure 3a). Changes affect mainly the 003:004 and 006:007 intensity ratios, differences being most significant for the Ba-SWy (Figure 3a), consistent with the high Z-number of Ba.

Sensitivity of XRD to interlayer species configuration. Figure 4 reports two sensitivity tests assessing the accuracy of XRD constraints on the interlayer H_2O content (Table 1) and on the position of maxima in the atomic H_2O profile derived from GCMC simulations (Figure 2a). The interlayer H_2O content is first modified by ± 10% keeping the distribution profile shown in Figure 2a. Significant misfit between calculated and experimental XRD intensity profiles arise both from the increasing and from the decrease of interlayer H_2O content (to 17.75 and 14.52 H_2O molecules p.f.u., respectively – Figure 4a).

Upon normalization to the 001 reflection, an increased interlayer H_2O content induces indeed an intensity increase of the 002, 004, and 006 reflections. Even a ± 5% variation of the interlayer H_2O content produces noticeable effect on calculated profiles. In the second test, the interlayer H_2O content was kept unchanged but the distribution profile shown in Figure 2a was stretched along the *z*-axis thus modifying the position of density maxima, and more specifically that of the two discrete and sharp ones at ~2.7 Å from the 2:1 layer. Upon normalization to the 001 reflection, a stretch of the distribution profile inducing a shift of these two density maxima by 0.1 Å results in severe misfits between calculated and experimental XRD profiles (Figure 4b). A similar effect was reported by Ferrage et al. (2011) to result from the 0.15 Å positional shift of the two main planes of H_2O molecules in 2W saponites. Both tests support the accuracy of GCMC configurations computed in the present study, and allow gaining further insights into the interactions of interlayer cations and H_2O molecules with the 2:1 layer.

Configuration of interlayer H_2O and cations in 3W montmorillonite

Pioneering XRD studies of H_2O structure in hydrated montmorillonite (including the 3W state) led to the hypothesis of several planes of interlayer H_2O molecules (Nagelschmidt 1936; Bradley et al. 1937; Hendricks and Merrill 1938; Mooney et al. 1952; Walker 1955). In these models, H_2O molecules form a pseudo-hexagonal planar network, each plane being composed of about 4 to 6 H_2O molecules p.f.u., the intercalation of one additional plane increasing the layer-to-layer distance by ~3 Å. Although still considered, these models differ significantly from the GCMC configurations computed in the present study. Oxygen and hydrogen density profiles reveal indeed two discrete planes of H_2O molecules whereas the "third" plane, which incorporates most of interlayer H_2O molecules, appears broad and poorly defined (Figure 2a). Contrasting to lower hydration states, the 3W hydration state (d_{001} = 18-19 Å) cannot be described simply by the juxtaposition of three similar planes of H_2O molecules, each ~3 Å thick, and the origin for the stability of the 3W state at ~18.5 Å needs to be sought elsewhere. A possible alternative for the existence of a discrete 3W hydration state is the influence of cations and more specifically local cation-water-clay interactions. Consistently, de La Calle and Suquet (1988) showed that the different d_{001} values observed for Ca-saturated vermiculite when increasing RH (14.66 and 14.92 Å) were related to distinct configurations of cation hydration shells and contrasting numbers of coordinating H_2O molecules. In addition, these authors determined that layer stacking mode was modified together with the change in hydration shell configuration. The existence of two stable 2W states for Ca-vermiculite was thus interpreted as resulting from the fine interactions between cations, H_2O molecules from their hydration shells, and the 2:1 surfaces, rather than from the steady filling of H_2O planes, as considered at the time. Within this context, molecular simulations thus represent especially relevant probes of local interactions between cations and coordinating H_2O molecules to refine our understanding of the interlayer structure of 3W smectites. The radial distribution function ($g(r)$) of cation-oxygen distances and related number of coordinating H_2O molecules ($N_{H2O}(r)$) are thus plotted in Figure 5. The number of H_2O molecules belonging to the first and second hydration shells (1HS and 2HS, respectively) can be derived from the $N_{H2O}(r)$ values on its first and second plateaus (Figure 5, Table 2).

Configuration of the first and second hydration shells. The average cation-H_2O distance in 1HS ranges from 2.16-2.79 Å (Mg-SWy and Ba-SWy, respectively – Table 2), and is consistent with cation radii (Shannon 1976). The associated number of H_2O molecules in 1HS obtained for the different cations (Table 2) vary from 5.74-9.34 H_2O molecules per cation (Na-SWy and Ba-SWy, respectively – Table 2), consistent with literature data on the hydration of sodium (Barnett and Landman 1993; Obst and Bradaczek 1996; Allen et al. 2000; Titiloye and Skipper 2000; White et al. 2000; Carrillo-Tripp et al. 2003; Smirnov and Trostin 2007; Mahler and Persson 2012; Morrow et al. 2013), magnesium (Peschke et al. 1998; Boero et al. 2002; Ikeda et al. 2007; Waluyo et al. 2011), calcium (Skipper et al. 1994; Jalilehvand et al. 2001) and barium (Peschke et al. 1998) in solution. Cation-clay and H_2O-clay interactions, and consequently confinement, thus appear to have a minor influence on H_2O molecules from the 1HS. Differentiation of these H_2O molecules (Figures 6a and 7) allows identifying three types of H_2O molecules. The first type includes H_2O molecules from 1HS that are located close to the interlayer mid-plane (Figures 6a and 7). H_2O molecules of the second type define the atomic density maxima at ~2.7 Å from the 2:1 layer surfaces (Figures 2a and 6a). This value, similar for all samples, is consistent both with the formation of strong H-bonds with surface oxygens from the 2:1 layer and with X-ray reflectivity results (Brown and Sturchio 2002; Fenter and Sturchio 2004; Lee et al. 2007) and indicates the presence of two planes of H_2O molecules wetting the 2:1 layer surfaces. Finally, H_2O molecules of the third type define the plateau between the previous two planes and essentially fill interlayer voids, further from the 2:1 layer surface. A similar analysis is possible for H_2O molecules from 2HS that define the diffuse maximum at 3.5-5.5 Å on the radial distribution function of cation-oxygen distances (Figure 5, Table 2). In contrast to 1HS, the number of H_2O molecules belonging to 2HS is similar for all samples within a narrow range of 13.7-15.7 molecules per cation (Table 2). The reduced scatter, compared to 1HS, suggests a minor influence of the cation radii. Comparison of atomic density profiles corresponding to H_2O molecules from 1HS and 2HS (Figures 6a and 6b, respectively) indicate that the latter belong to the second and third types of H_2O molecules, with a significant fraction of H_2O molecules from 2HS also wetting the 2:1 layer surface (Figures 6b and 8). Although reduced, the number of H_2O molecules of the second type not belonging to interlayer cation hydration spheres remains important together with the number of H_2O molecules filling interlayer voids with the persistence of the uniform plateau (solid gray lines – Figure 6b). In addition, a fraction of H_2O from 2HS is shared between cations (Figure 8), and more specifically so for Na-SWy owing to the twofold number of monovalent cations. Additional calculations allowed quantifying the fraction of shared H_2O molecules both from 1HS and 2HS (Table 2). In particular, it is possible to note that the fraction of H_2O molecules hydrating two cations remains limited to a few percent for divalent cations, this proportion increasing to ~20% for monovalent Na, which even shares a limited fraction of H_2O molecules from 1HS (Table 2).

Origin of the stability of the montmorillonite 3W hydrate. A detailed analysis of H_2O molecules in cation 1HS and 2HS allows drawing a general picture of interlayer H_2O configuration in 3W montmorillonite and to decipher factors ruling its stability in layer-to-layer distance at ~19 Å (Table 1). Analysis of H_2O molecules from 1HS does not provide any insight into the relation between hydrated cations and the clay surface, the distance involved being too large (Figure 7). In addition, contrasting configurations reported for 1HS both in terms of cation-H_2O molecule distance and of number of coordinating H_2O molecules (Table 2) cannot account for the similarity of d_{001} values measured for the different interlayer cations (Table 1). On the contrary, detailed analysis of H_2O molecules from 2HS reveals that a significant fraction of these molecules are involved also in the wetting of the 2:1 layer surface (Figure 8). In addition, shared H_2O molecules from 2HS ensure the formation of a 2D network. Both effects are similar to those proposed by De La Calle and

Suquet (1988) as being responsible for the stability of 1W and 2W hydrates in vermiculite and saponite. The limited contrast, both in terms of cation-H_2O molecule distance and of number of coordinating H_2O molecules, between the 2HS of the various cations investigated yield similar layer-to-layer distances (Tables 1 and 2). This hypothesis is consistent with contrasting proportions of H_2O molecules from 1HS and 2HS, compared to other types of H_2O molecules, between the different cations despite similar d_{001} values. For example, the proportion of H_2O molecules not bound to interlayer Na is strongly reduced compared to other samples saturated with divalent cations (Figures 6b). Second and third types of H_2O molecules thus likely contribute only to wetting the 2:1 layer surface or to filling interlayer voids, respectively, whereas layer-to-layer distance is controlled by H_2O molecules from 2HS. Note however that layer-to-layer distance of 3W montmorillonite will likely vary with overall H_2O contents as previously reported for 1W and 2W hydrates (Ferrage et al. 2005b, 2007a, 2007c). Finally, the importance of H_2O molecule sharing in Na-SWy allows hypothesizing that stable hydrates with higher layer-to-layer distances could exist as proposed by Bradley et al. (1937) for a Na-montmorillonite at ~21.4 Å.

Simplified interlayer model for XRD simulation of 3W hydrates

Although comparison of experimental and computational data validates the simulated interlayer configurations of 3W montmorillonite for a variety of interlayer cations, GCMC simulations cannot be used systematically to quantitatively analyze XRD data from a large number of samples. The latter analysis relies essentially on XRD profile modeling of 00*l* reflections and requires a realistic and simplified description of interlayer structure (Moore and Reynolds 1997). Such a description considers usually one or several planes of H_2O

molecules and/or cations characterized by i) a *z*-coordinate along the c* axis, ii) a quantity of atoms in this plane, and iii) a Debye-Waller factor (B) accounting for the positional disorder of interlayer species. The B factor thus accounts for the distribution of atoms perpendicular to the layer plane described by atomic density profiles derived from Monte Carlo simulations. When using the B parameter, this physical distribution of species along the c*-axis is approximated by a Gaussian function whose FWHM is (Shashikala et al. 1993; Dazas et al 2013):

$$FWHM = \frac{\sqrt{B}\sqrt{\mathrm{Ln}(2)}}{\pi} \qquad \text{(Eq. 3)}$$

The GCMC configuration computed for 3W hydrates (Figure 2b) can thus be approximated by a model with a few planes of interlayer cations and H_2O molecules with contrasting B values (Figures 2c and 2d). The two maxima of the atomic density profiles corresponding to H_2O molecules of the second type can be described by a set of two planes, symmetrical with respect to the interlayer mid-plane, and located at 3.35-3.60 Å from the interlayer mid-plane. Taking into account the variable d_{001} values, these planes are systematically located at ~2.7 Å from the 2:1 layer surface, in agreement with X-ray reflectivity results for the presence of H_2O molecules wetting clay surfaces (Brown and Sturchio 2002; Fenter and Sturchio 2004; Lee et al. 2007). Each of these two planes contains 3.0-3.2 H_2O molecules p.f.u., that is ~20% of the total interlayer H_2O content, with a B parameter of ~10-15 Å² (Table 3, Figure 2c). All attempts to approximate the plateau of the oxygen density profile with a single contribution proved unsuccessful, as the B value associated to such a single plane would be extremely high leading to H_2O molecules being too close to the 2:1 layer surface, or even passing it. A second set of two planes, symmetrical with respect to the interlayer mid-plane, was thus considered at 1.20-1.35 Å from the interlayer mid-plane. This distance corresponds to 21% of that from the interlayer mid-plane to the 2:1 layer surface. Each of these two planes contains 4.2-4.8 H_2O molecules p.f.u., that is ~30% of the total interlayer H_2O content, with a B parameter of ~100 Å² (Table 3, Figure 2c). A set of two planes, symmetrical with respect to the interlayer mid-plane, was considered for interlayer cations, as such a doublet allowed better fits to XRD data, specifically for Ba-SWy, compared to a single plane centered on the interlayer mid-plane (data not shown). These planes are located at 0.00-1.20 Å from the interlayer mid-plane, B values depending on the nature of the interlayer cation (20-45 Å^2 – Table 3). The positive correlation between the cation ionic potential (valence over ionic radius ratio) and the distance from interlayer cations to the surface of the 2:1 layer (Figure 9) allows approximating the actual position of cationic planes for species not reported in the present study. This simplified structure model of 3W smectite interlayer space allows reproducing satisfactorily the XRD data for all samples investigated (Figure 3b), and can thus be used for routine quantitative analysis of XRD data recorded from smectite-bearing clayey samples recorded at high H_2O activity. Table 4 thus recaps relevant parameters of this simplified structure model for 3W smectite in an effort to complement the structure model of 0W, 1W, and 2W proposed by Moore and Reynolds (1997) and further refined by Ferrage et al. (2005b, 2005c, 2007a, 2007b, 2007c, 2010).

IMPLICATIONS

A key issue in assessing the safety of municipal and nuclear waste disposal is the ability to model solute transport in clay porous media under near-saturated water condition, and, possibly, constrained confinement. In such a context inter-particle porosity controls, at least in part, the diffusion of anions, cations, and H_2O whereas interlayer porosity influences also the diffusion of the latter two species (Pavlović and Stamatović 1992; Melkior et al. 2005; 2009). Inter-particle porosity can be estimated from the apparent dry bulk density, the extent of crystalline swelling, and the total constrained volume (Fernández and Rivas 2005; Bourg et al. 2006; Van Loon et al. 2007; Muurinen 2009; Holmboe et al. 2012). Within this scope, the structure model of 3W smectite proposed in the present study will allow quantifying crystalline swelling by XRD under near-saturated conditions, thus providing further constraints on the extent of crystalline swelling and on the organization and mobility of interlayer H_2O molecules. In addition, interlayer H_2O contents refined in the present study for high H_2O activity conditions allow a stronger control on the calculation of H_2O present in the inter-particle porosity. This additional control complements previous studies devoted to quantifying the different types of H_2O molecules in swelling clay porous media (H_2O molecules in 1W or 2W layers, and pore water – Ferrage et al. 2010; Dazas et al. 2013). Ferrage et al. (2010) showed for saponites that the water content derived from XRD profile modeling was consistent with total water content for RH values < 70%. For higher RH values, these authors assigned the increase in total water content to sorption of capillary water in the pore network owing to stability of the 2W hydrate, most likely as the result of tetrahedral charge location.

ACKNOWLEDGMENTS

The CNRS interdisciplinary défi Needs, through its "MiPor" program, and the ANR "Jeunes Chercheurs" program (contract No. ANR-09-JCJC-0106-PorousClay) are thanked for the financial support provided to the present study.

REFERENCES

Åqvist, J. (1990) Ion-water interaction potentials derived from free energy perturbation simulations. The Journal of Physical Chemistry, 94, 8021-8024.

Adams, D.J. (1974) Chemical potential of hard-sphere fluids by Monte Carlo methods. Molecular Physics, 28, 1241-1252.

-. (1975) Grand canonical ensemble Monte Carlo for a Lennard-Jones fluid. Molecular Physics, 29, 307-311.

Allen, M.P. and Tildesley, D.J. (1994) Computer Simulation of Liquids, 412 p. Oxford University Press.

Allen, T.W., Bliznyuk, A., Rendell, A.P., Kuyucak, S., and Chung, S.H. (2000) The potassium channel: Structure, selectivity and diffusion. The Journal of Chemical Physics, 112, 8191-8204.

Appelo, C.A.J., Van Loon, L.R., and Wersin, P. (2010) Multicomponent diffusion of a suite of tracers (HTO, Cl, Br, I, Na, Sr, Cs) in a single sample of Opalinus Clay. Geochimica et Cosmochimica Acta, 74, 1201-1219.

Baeyens, B. and Bradbury, M.H. (1997) A mechanistic description of Ni and Zn sorption on Na-montmorillonite Part I: Titration and sorption measurements. Journal of Contaminant Hydrology, 27, 199-222.

Barnett, R.N. and Landman, U. (1993) Hydration of sodium in water clusters. Physical Review Letters, 70, 1775-1778.

Berend, I., Cases, J.-M., Francois, M., Uriot, J.-P., Michot, L., Masion, A., and Thomas, F. (1995) Mechanism of adsorption and sesorption of water vapor by homoionic montmorillonites: 2. The Li^+, Na^+, K^+, Rb^+, and Cs^+-exchanged Forms. Clays and Clay Minerals, 43, 324-336.

Berendsen, H.J.C., Postma, J.P.M., Van Gunsteren, W.F., and Hermans, J. (1981) Interaction models for water in relation to protein hydration. Intermolecular Forces, 11, 331-342.

Bittelli, M., Valentino, R., Salvatorelli, F., and Rossi Pisa, P. (2012) Monitoring soil-water and displacement conditions leading to landslide occurrence in partially saturated clays. Geomorphology, 173–174, 161-173.

Boek, E.S., Coveney, P.V., and Skipper, N.T. (1995a) Monte Carlo Molecular Modeling Studies of Hydrated Li-, Na-, and K-Smectites: Understanding the Role of Potassium as a Clay Swelling Inhibitor. Journal of the American Chemical Society, 117, 12608-12617.

-. (1995b) Molecular Modeling of Clay Hydration: A Study of Hysteresis Loops in the Swelling Curves of Sodium Montmorillonites. Langmuir, 11, 4629-4631.

Boero, M., Terakura, K., and Tateno, M. (2002) Catalytic Role of Metal Ion in the Selection of Competing Reaction Paths: A First Principles Molecular Dynamics Study of the Enzymatic Reaction in Ribozyme. Journal of the American Chemical Society, 124, 8949-8957.

Boullier, A.-M., Yeh, E.-C., Boutareaud, S., Song, S.-R., and Tsai, C.-H. (2009) Microscale anatomy of the 1999 Chi-Chi earthquake fault zone. Geochemistry Geophysics Geosystems, 10, Q03016, doi:10.1029/2008GC002252.

Bouma, J., Jongerius, A., Boersma, O., Jager, A., and Schoonderbeek, D. (1977) Function of Different Types of Macropores During Saturated Flow Through 4 Swelling Soil Horizons. Soil Science Society of America Journal, 41, 945-950.

Bourg, I.C., Sposito, G., and Bourg, A.C.M. (2006) Tracer diffusion in compacted, water-saturated bentonite. Clays and Clay Minerals, 54, 363-374.

Boutareaud, S., Calugaru, D.-G., Han, R., Fabbri, O., Mizoguchi, K., Tsutsumi, A., and Shimamoto, T. (2008) Clay-clast aggregates: A new textural evidence for seismic fault sliding? Geophysical Research Letters, 35, L05302, doi:10.1029/2007GL032554.

Bradley, W.F., Grim, R.E., and Clark, G.L. (1937) A study of the behavior of montmorillonite upon wetting. Zeitschrift für Kristallographie, 97, 216-222.

Brown, G.E. and Sturchio, N.C. (2002) An Overview of Synchrotron Radiation Applications to Low Temperature Geochemistry and Environmental Science. In P. Fenter, and N.C. Sturchio, Eds., Applications of Synchrotron Radiation in Low-Temperature Geochemistry and Environmental Sciences, 49, p. 1-115. Mineralogical Society of America, Chantilly, Va.

Burst, J.F. (1969) Diagenesis of Gulf Coast clayey sediments and its possible relation to petroleum migration. American Association of Petroleum Geologists Bulletin, 53, 73-93.

Carrillo-Tripp, M., Saint-Martin, H., and Ortega-Blake, I. (2003) A comparative study of the hydration of Na^+ and K^+ with refined polarizable model potentials. The Journal of Chemical Physics, 118, 7062-7073.

Cases, J.M., Berend, I., Besson, G., Francois, M., Uriot, J.P., Thomas, F., and Poirier, J.E. (1992) Mechanism of adsorption and desorption of water vapor by homoionic montmorillonite. 1. The sodium-exchanged form. Langmuir, 8, 2730-2739.

Cases, J.M., Berend, I., Francois, M., Uriot, J.P., Michot, L.J., and Thomas, F. (1997) Mechanism of adsorption and desorption of water vapor by homoionic montmorillonite: 3. The Mg^{2+}, Ca^{2+}, Sr^{2+}, and Ba^{2+} exchanged forms. Clays and Clay Minerals, 45, 8-22.

Chang, F.-R.C., Skipper, N.T., and Sposito, G. (1995) Computer Simulation of Interlayer Molecular Structure in Sodium Montmorillonite Hydrates. Langmuir, 11, 2734-2741.

-. (1997) Monte Carlo and Molecular Dynamics Simulations of Interfacial Structure in Lithium-Montmorillonite Hydrates. Langmuir, 13, 2074-2082.

Cygan, R.T., Liang, J.J., and Kalinichev, A.G. (2004) Molecular models of hydroxide, oxyhydroxide, and clay phases and the development of a general force field. The Journal of Physical Chemistry B, 108, 1255-1266.

Dazas, B., Lanson, B., Breu, J., Robert, J.-L., Pelletier, M., and Ferrage, E. (2013) Smectite fluorination and its impact on interlayer water content and structure: A way to fine tune the hydrophilicity of clay surfaces? Microporous and Mesoporous Materials, 181, 233-247.

De La Calle, C. and Suquet, H. (1988) Vermiculite. In S.W. Bailey, Ed., Hydrous phyllosilicates: (exclusive of micas), 19, p. 455-496. Mineralogical Society of America, Chantilly, Virginia.

Delville, A. (1991) Modeling the clay-water interface. Langmuir, 7, 547-555.

Drits, V.A. and Sakharov, B.A. (1976) X-ray structural analysis of mixed-layer minerals, 256 p. Nauka, Moscow.

Drits, V.A. and Tchoubar, C. (1990) X-ray diffraction by disordered lamellar structures: Theory and applications to microdivided silicates and carbons, 371 p. Springer-Verlag, Berlin.

Fenter, P. and Sturchio, N.C. (2004) Mineral–water interfacial structures revealed by synchrotron X-ray scattering. Progress in Surface Science, 77, 171-258.

Fernández, A.M. and Rivas, P. (2005) Analysis and distribution of waters in the compacted FEBEX bentonite: pore water chemistry and adsorbed water properties. In E.E. Alonso, and A. Ledesma, Eds., Advances in Understanding Engineered Clay Barriers, p. 257-275.

Ferrage, E., Lanson, B., Malikova, N., Plançon, A., Sakharov, B.A., and Drits, V.A. (2005c) New Insights on the Distribution of Interlayer Water in Bi-Hydrated Smectite from X-ray Diffraction Profile Modeling of 00l Reflections. Chemistry of Materials, 17, 3499-3512.

Ferrage, E., Lanson, B., Sakharov, B.A., and Drits, V.A. (2005b) Investigation of smectite hydration properties by modeling experimental X-ray diffraction patterns: Part I. Montmorillonite hydration properties. American Mineralogist, 90, 1358-1374.

Ferrage, E., Tournassat, C., Rinnert, E., and Lanson, B. (2005a) Influence of pH on the interlayer cationic composition and hydration state of Ca-montmorillonite: Analytical chemistry, chemical modelling and XRD profile modelling study. Geochimica et Cosmochimica Acta, 69, 2797-2812.

Ferrage, E., Kirk, C.A., Cressey, G., and Cuadros, J. (2007c) Dehydration of Ca-montmorillonite at the crystal scale. Part I: Structure evolution. American Mineralogist, 92, 994-1006.

-. (2007a) Dehydration of Ca-montmorillonite at the crystal scale. Part 2. Mechanisms and kinetics. American Mineralogist, 92, 1007-1017.

Ferrage, E., Lanson, B., Sakharov, B.A., Geoffroy, N., Jacquot, E., and Drits, V.A. (2007b) Investigation of dioctahedral smectite hydration properties by modeling of X-ray diffraction profiles: Influence of layer charge and charge location. American Mineralogist, 92, 1731-1743.

Ferrage, E., Lanson, B., Michot, L.J., and Robert, J.-L. (2010) Hydration Properties and Interlayer Organization of Water and Ions in Synthetic Na-Smectite with Tetrahedral Layer Charge. Part

1. Results from X-ray Diffraction Profile Modeling. The Journal of Physical Chemistry C, 114, 4515-4526.

Ferrage, E., Sakharov, B.A., Michot, L.J., Delville, A., Bauer, A., Lanson, B., Grangeon, S., Frapper, G., Jimenez-Ruiz, M., and Cuello, G.J. (2011) Hydration Properties and Interlayer Organization of Water and Ions in Synthetic Na-Smectite with Tetrahedral Layer Charge. Part 2. Toward a Precise Coupling between Molecular Simulations and Diffraction Data. The Journal of Physical Chemistry C, 115, 1867-1881.

Fu, M.H., Zhang, Z.Z., and Low, P.F. (1990) Changes in the properties of a montmorillonite-water system during the adsorption and desorption of water; hysteresis. Clays and Clay Minerals, 38, 485-492.

Gates, W.P., Bouazza, A., and Churchman, G.J. (2009) Bentonite Clay Keeps Pollutants at Bay. Elements, 5, 105-110.

Glaus, M.A., Baeyens, B., Bradbury, M.H., Jakob, A., Van Loon, L.R., and Yaroshchuk, A. (2007) Diffusion of ^{22}Na and ^{85}Sr in montmorillonite : Evidence of interlayer diffusion being the dominant pathway at high compaction. Environmental Science & Technology, 41, 478-485.

Greathouse, J.A. and Storm, E.W. (2002) Calcium hydration on montmorillonite clay surfaces studied by Monte Carlo simulation. Molecular Simulation, 28, 633-647.

Heinz, H., Koerner, H., Anderson, K.L., Vaia, R.A., and Farmer, B.L. (2005) Force Field for Mica-Type Silicates and Dynamics of Octadecylammonium Chains Grafted to Montmorillonite. Chemistry of Materials, 17, 5658-5669.

Henderson, M.A. (2002) The interaction of water with solid surfaces: fundamental aspects revisited. Surface Science Reports, 46, 1-308.

Hendricks, S.B. and Merrill, E.J. (1938) Crystal structure of vermiculites and mixed vermiculite-chlorites. American Mineralogist, 23, 851-862.

Heyes, D.M. (1994) Pressure tensor of partial-charge and point-dipole lattices with bulk and surface geometries. Physical Review B, 49, 755-764.

Holmboe, M., Wold, S., and Jonsson, M. (2012) Porosity investigation of compacted bentonite using XRD profile modeling. Journal of Contaminant Hydrology, 128, 19-32.

Ikeda, T., Boero, M., and Terakura, K. (2007) Hydration properties of magnesium and calcium ions from constrained first principles molecular dynamics. The Journal of Chemical Physics, 127, 074503.

Jalilehvand, F., Spångberg, D., Lindqvist-Reis, P., Hermansson, K., Persson, I., and Sandström, M. (2001) Hydration of the Calcium Ion. An EXAFS, Large-Angle X-ray Scattering, and Molecular Dynamics Simulation Study. Journal of the American Chemical Society, 123, 431-441.

Jiménez-Ruiz, M., Ferrage, E., Delville, A., and Michot, L.J. (2012) Anisotropy on the Collective Dynamics of Water Confined in Swelling Clay Minerals. The Journal of Physical Chemistry A, 116, 2379-2387.

Karaborni, S., Smit, B., Heidug, W., Urai, J., and Oort, E.v. (1996) The Swelling of Clays: Molecular Simulations of the Hydration of Montmorillonite. Science, 271, 1102-1104.

Kawamura, K., Ichikawa, Y., Nakano, M., Kitayama, K., and Kawamura, H. (1999) Swelling properties of smectite up to 90°C: In situ X-ray diffraction experiments and molecular dynamic simulations. Engineering Geology, 54, 75-79.

Lee, S.S., Nagy, K.L., and Fenter, P. (2007) Distribution of barium and fulvic acid at the mica–solution interface using in-situ X-ray reflectivity. Geochimica et Cosmochimica Acta, 71, 5763-5781.

Mahler, J. and Persson, I. (2012) A Study of the Hydration of the Alkali Metal Ions in Aqueous Solution. Inorganic Chemistry, 51, 425-438.

Malikova, N., Cadène, A., Marry, V., Dubois, E., and Turq, P. (2006) Diffusion of water in clays on the microscopic scale: modeling and experiment. The Journal of Physical Chemistry B, 110, 3206-3214.

Malikova, N., Cadène, A., Dubois, E., Marry, V., Durand-Vidal, S., Turq, P., Breu, J., Longeville, S., and Zanotti, J.M. (2007) Water Diffusion in a Synthetic Hectorite Clay Studied by Quasi-elastic Neutron Scattering. The Journal of Physical Chemistry C, 111, 17603-17611.

Malikova, N., Dubois, E., Marry, V., Rotenberg, B., and Turq, P. (2010) Dynamics in Clays - Combining Neutron Scattering and Microscopic Simulation. Zeitschrift Fur Physikalische Chemie, 224, 153-181.

Marry, V. and Turq, P. (2003) Microscopic Simulations of Interlayer Structure and Dynamics in Bihydrated Heteroionic Montmorillonites. The Journal of Physical Chemistry B, 107, 1832-1839.

Marry, V., Dubois, E., Malikova, N., Durand-Vidal, S., Longeville, S.p., and Breu, J. (2011) Water Dynamics in Hectorite Clays: Infuence of Temperature Studied by Coupling Neutron Spin Echo and Molecular Dynamics. Environmental Science & Technology, 45, 2850-2855.

Matsuda, T., Omura, K., Ikeda, R., Arai, T., Kobayashi, K., Shimada, K., Tanaka, H., Tomita, T., and Hirano, S. (2004) Fracture-zone conditions on a recently active fault: insights from mineralogical and geochemical analyses of the Hirabayashi NIED drill core on the Nojima fault, southwest Japan, which ruptured in the 1995 Kobe earthquake. Tectonophysics, 378, 143-163.

Meleshyn, A. and Bunnenberg, C. (2005) Swelling of Na/Mg-montmorillonites and hydration of interlayer cations: A Monte Carlo study. The Journal of Chemical Physics, 123, p074509.

Melkior, T., Yahiaoui, S., Motellier, S., Thoby, D., and Tevissen, E. (2005) Cesium sorption and diffusion in Bure mudrock samples. Applied Clay Science, 29, 172-186.

Melkior, T., Yahiaoui, S., Thoby, D., Motellier, S., and Barthès, V. (2007) Diffusion coefficients of alkaline cations in Bure mudrock. Physics and Chemistry of the Earth, Parts A/B/C, 32, 453-462.

Melkior, T., Gaucher, E.C., Brouard, C., Yahiaoui, S., Thoby, D., Clinard, C., Ferrage, E., Guyonnet, D., Tournassat, C., and Coelho, D. (2009) Na^+ and HTO diffusion in compacted bentonite: Effect of surface chemistry and related texture. Journal of Hydrology, 370, 9-20.

Mermut, A.R., Lagaly, G., and others. (2001) Baseline studies of the clay minerals society source clays: layer-charge determination and characteristics of those minerals containing 2: 1 layers. Clays and Clay Minerals, 49, 393-397.

Michot, L., Maslon, I.A., and Thomas, F. (1995) Mechanism of adsorption and desorption of water vapor by homoionic montmorillonites: 2. The Li^+, Na^+, K^+, Rb^+, and Cs^+-exchanged forms. Clays and Clay Minerals, 43, 324-336.

Michot, L.J., Delville, A., Humbert, B., Plazanet, M., and Levitz, P. (2007) Diffusion of Water in a Synthetic Clay with Tetrahedral Charges by Combined Neutron Time-of-Flight Measurements and Molecular Dynamics Simulations. The Journal of Physical Chemistry C, 111, 9818-9831.

Michot, L.J., Ferrage, E., Jimenez-Ruiz, M., Boehm, M., and Delville, A. (2012) Anisotropic Features of Water and Ion Dynamics in Synthetic Na- and Ca-Smectites with Tetrahedral Layer Charge. A Combined Quasi-elastic Neutron-Scattering and Molecular Dynamics Simulations Study. The Journal of Physical Chemistry C, 116, 16619-16633.

Mooney, R.W., Keenan, A.G., and Wood, L.A. (1952) Adsorption of Water Vapor by Montmorillonite. II. Effect of Exchangeable Ions and Lattice Swelling as Measured by X-Ray Diffraction. Journal of the American Chemical Society, 74, 1371-1374.

Moore, D.M. and Reynolds, R.C. (1997) X-ray Diffraction and the Identification and Analysis of Clay Minerals, 378 p. Oxford University Press, Oxford.

Morrow, C.P., Yazaydin, A.Ö., Krishnan, M., Bowers, G.M., Kalinichev, A.G., and Kirkpatrick, R.J. (2013) Structure, energetics, and dynamics of smectite clay interlayer hydration: Molecular dynamics and metadynamics investigation of Na-hectorite. The Journal of Physical Chemistry C ,117, 5172-5187.

Muurinen, A. (2009) Studies on the chemical conditions and microstructure in the reference bentonites of alternative buffer materials project (ABM) in Äspö, 46 p. Posiva Oy, Eurajoki.

Nagelschmidt, G. (1936) On the lattice shrinkage and structure of montmorillonite. Zeitschrift für Kristallographie, 93, 481-487.

Norrish, K. (1954) The swelling of montmorillonite. Discussions of the Faraday Society, 18, 120-134.

Obst, S. and Bradaczek, H. (1996) Molecular Dynamics Study of the Structure and Dynamics of the Hydration Shell of Alkaline and Alkaline-Earth Metal Cations. The Journal of Physical Chemistry, 100, 15677-15687.

Oueslati, W., Mefath, M., Ben Rhaiem, H., and Amara, A.B. (2009) Cation Exchange Selectivity versus concentration of competing heavy metal cations (Pb^{2+}, Zn^{2+}): case of Na-montmorillonite. Physics Procedia, 2, 1059-1063.

Pavlović, L. and Stamatović, M. (1992) Effect of exchangeable cation on water diffusion in kaolinite. Applied Clay Science, 7, 313-322.

Peschke, M., Blades, A.T., and Kebarle, P. (1998) Hydration Energies and Entropies for Mg^{2+}, Ca^{2+}, Sr^{2+}, and Ba^{2+} from Gas-Phase Ion−Water Molecule Equilibria Determinations. The Journal of Physical Chemistry A, 102, 9978-9985.

Pons, C.H., Rousseaux, F., and Tchoubar, D. (1981a) Utilisation du rayonnement synchrotron en diffusion aux petits angles pour l'étude du gonflement des smectites: I Etude du système eau-montmorillonite-Na en fonction de la température. Clay Minerals, 16, 23-42.

-. (1981b) Utilisation du rayonnement synchrotron en diffusion aux petits angles pour l'étude du gonflement des smectites: II Etude du système eau-montmorillonite-Na en fonction de la température. Clay Minerals, 16, 23-42.

Porion, P., Al Mukhtar, M., Faugere, A.M., Pellenq, R.J.M., Meyer, S., and Delville, A. (2003) Water self-diffusion within nematic dispersions of nanocomposites: A multiscale analysis of ^1H pulsed gradient spin-echo NMR measurements. The Journal of Physical Chemistry B, 107, 4012-4023.

Porion, P., Faugère, A.M., and Delville, A. (2008) ^1H and ^7Li NMR Pulsed Gradient Spin Echo Measurements and Multiscale Modeling of the Water and Ionic Mobility within Aqueous Dispersions of Charged Anisotropic Nanoparticles. The Journal of Physical Chemistry C, 112, 11893-11900.

Rinnert, E., Carteret, C., Humbert, B., Fragneto-Cusani, G., Ramsay, J.D.F., Delville, A., Robert, J.-L., Bihannic, I., Pelletier, M., and Michot, L.J. (2005) Hydration of a Synthetic Clay with Tetrahedral Charges: A Multidisciplinary Experimental and Numerical Study. The Journal of Physical Chemistry B, 109, 23745-23759.

Sakharov, B.A. and Lanson, B. (2013) X-ray Identification of Mixed-Layer Structures. Modelling of Diffraction Effects. In F. Bergaya, and G. Lagaly, Eds., Handbook of Clay Science, 5B, p. 51-135. Elsevier, Amsterdam, Oxford.

Sánchez, F.t.G.l., Gimmi, T., Jurányi, F., Loon, L.V., and Diamond, L.W. (2009) Linking the Diffusion of Water in Compacted Clays at Two Different Time Scales: Tracer Through-Diffusion and Quasielastic Neutron Scattering. Environmental Science & Technology, 43, 3487-3493.

Sato, T., Watanabe, T., and Otsuka, R. (1992) Effects of layer charge, charge location, and energy change on expansion properties of dioctahedral smectites. Clays and Clay Minerals, 40, 103-113.

Shannon, R.D. (1976) Revised effective ionic radii and systematic studies of interatomic distances in halides and chalcogenides. Acta Crystallographica A, 32, 751-767.

Shashikala, H.D., Suryanarayana, S.V., and Nagender Naidu, S.V. (1993) Debye temperature and mean-square amplitudes of vibration of Ti 3Al alloys. Journal of Applied Crystallography, 26, 602-605.

Sing, K.S.W. (1982) Reporting physisorption data for gas/solid systems. Pure and Applied Chemistry, 54, 2201-2218.

Skipper, N.T., Soper, A.K., and Smalley, M.V. (1994) Neutron diffraction study of calcium vermiculite: hydration of calcium ions in a confined environment. The Journal of Physical Chemistry, 98, 942-945.

Skipper, N.T., Chang, F.R.C., and Sposito, G. (1995) Monte-carlo simulation of interlayer molecular-structure in swelling clay-minerals .1. Methodology. Clays and Clay Minerals, 43, 285-293.

Smirnov, P.R. and Trostin, V.N. (2007) Structure of the nearest surrounding of the Na+ ion in aqueous solutions of its salts. Russian Journal of General Chemistry, 77, 844-850.

Smith, D.E., Wang, Y., Chaturvedi, A., and Whitley, H.D. (2006) Molecular Simulations of the Pressure, Temperature, and Chemical Potential Dependencies of Clay Swelling. The Journal of Physical Chemistry B, 110, 20046-20054.

Stucki, J., Golden, D., and Roth, C. (1984) Effects of Reduction and Reoxidation of Structural Iron on the Surface-Charge and Dissolution of Dioctahedral Smectites. Clays and Clay Minerals, 32, 350-356.

Suzuki, S., Sato, H., Ishidera, T., and Fujii, N. (2004) Study on anisotropy of effective diffusion coefficient and activation energy for deuterated water in compacted sodium bentonite. Journal of Contaminant Hydrology, 68, 23-37.

Takahashi, A., Fung, D.W.H., and Jardine, F. (2005) Swelling effects on mechanical behaviour of natural London Clay. Proceedings of the 16th International Conference on Soil Mechanics and Foundation Engineering, 2, p. 443-446.

Tambach, T.J., Hensen, E.J.M., and Smit, B. (2004) Molecular Simulations of Swelling Clay Minerals. The Journal of Physical Chemistry B, 108, 7586-7596.

Tambach, T.J., Bolhuis, P.G., Hensen, E.J.M., and Smit, B. (2006) Hysteresis in clay swelling induced by hydrogen bonding: accurate prediction of swelling states. Langmuir, 22, 1223-1234.

Tao, L., Xiao-Feng, T., Yu, Z., and Tao, G. (2010) Swelling of K^+, Na^+ and Ca^{2+}-montmorillonites and hydration of interlayer cations: a molecular dynamics simulation. Chinese Physics B, 19, 109101.

Tertre, E., Berger, G., Castet, S., Loubet, M., and Giffaut, E. (2005) Experimental sorption of Ni^{2+}, Cs^+ and Ln^{3+} onto a montmorillonite up to 150°C. Geochimica et Cosmochimica Acta, 69, 4937-4948.

Tertre, E., Berger, G., Simoni, E., Castet, S., Giffaut, E., Loubet, M., and Catalette, H. (2006) Europium retention onto clay minerals from 25 to 150 °C: Experimental measurements, spectroscopic features and sorption modelling. Geochimica et Cosmochimica Acta, 70, 4563-4578.

Tertre, E., Ferrage, E., Bihannic, I., Michot, L.J., and Prêt, D. (2011a) Influence of the ionic strength and solid/solution ratio on Ca(II)-for-Na^+ exchange on montmorillonite. Part 2: Understanding the effect of the m/V ratio. Implications for pore water composition and element transport in natural media. Journal of Colloid and Interface Science, 363, 334-347.

Tertre, E., Pret, D., and Ferrage, E. (2011b) Influence of the ionic strength and solid/solution ratio on Ca(II)-for-Na^+ exchange on montmorillonite. Part 1: Chemical measurements, thermodynamic modeling and potential implications for trace elements geochemistry. Journal of Colloid and Interface Science, 353, 248-256.

Titiloye, J.O. and Skipper, N.T. (2000) Computer simulation of the structure and dynamics of methane in hydrated Na-smectite clay. Chemical Physics Letters, 329, 23-28.

Tournassat, C., Ferrage, E., Poinsignon, C., and Charlet, L. (2004) The titration of clay minerals: II. Structure-based model and implications for clay reactivity. Journal of Colloid and Interface Science, 273, 234-246.

Turner, G.D., Zachara, J.M., McKinley, J.P., and Smith, S.C. (1996) Surface-charge properties and UO_2^{2+} adsorption of a subsurface smectite. Geochimica et Cosmochimica Acta, 60, 3399-3414.

Van Loon, L.R., Soler, J.M., Müller, W., and Bradbury, M.H. (2004) Anisotropic diffusion in layered argillaceous rocks: a case study with Opalinus Clay. Environmental Science & Technology, 38, 5721-5728.

Van Loon, L.R., Baeyens, B., and Bradbury, M.H. (2005) Diffusion and retention of sodium and strontium in Opalinus clay: Comparison of sorption data from diffusion and batch sorption measurements, and geochemical calculations. Applied Geochemistry, 20, 2351-2363.

Van Loon, L.R., Glaus, M.A., and Müller, W. (2007) Anion exclusion effects in compacted bentonites: Towards a better understanding of anion diffusion. Applied Geochemistry, 22, 2536-2552.

Vrolijk, P. (1990) On the mechanical role of smectite in subduction zones. Geology, 18, 703-707.

Walker, G.F. (1955) The Mechanism of Dehydration of Mg-Vermiculite. Clays and Clay Minerals, 4, 101-115.

Waluyo, I., Huang, C., Nordlund, D., Bergmann, U., Weiss, T.M., Pettersson, L.G.M., and Nilsson, A. (2011) The structure of water in the hydration shell of cations from X-ray, Raman and small angle X-ray scattering measurements. The Journal of Chemical Physics, 134, 064513.

White, J.A., Schwegler, E., Galli, G., and Gygi, F. (2000) The solvation of Na^+ in water: First-principles simulations. The Journal of Chemical Physics, 113, 4668-4673.

Young, D.A. and Smith, D.E. (2000) Simulations of Clay Mineral Swelling and Hydration: Dependence upon Interlayer Ion Size and Charge. The Journal of Physical Chemistry B, 104, 9163-9170.

Zeng, Q.H., Yu, A.B., Lu, G.Q., and Standish, R.K. (2004) Molecular Dynamics Simulation of the Structural and Dynamic Properties of Dioctadecyldimethyl Ammoniums in Organoclays. The Journal of Physical Chemistry B, 108, 10025-10033.

TABLES

Table 1. Experimental parameters of 3W montmorillonite.

Sample	d_{001} value (Å)	ξ parameter (Å)	Layer abundance 3W/2W (%)
Mg-SWy	19.23	0.057	98/2
Ca-SWy	18.93	0.062	98/2
Ba-SWy	18.90	0.042	97/3
Na-SWy	18.73	0.056	92/8

Note: The layer-to-layer distance (d_{001}) and the relative contents of 3W and 2W layers were determined from the simulation of XRD data. The rationality estimate (ξ) was calculated as the standard deviation of $l \times d_{00l}$ values (in Å) for the ten 00*l* reflections measurable over the 2-50° 2θ range.

Table 2. Content and local environment of interlayer H_2O molecules from the first (1HS) and second (2HS) cation hydration shells deduced from GCMC simulations.

		1HS				2HS		
Sample	Water content (p.f.u.)	Cat.-H_2O distance (Å)	nH_2O (per cation)	nH_2O shared (p.f.u.)	Ionic rad. (Å) / coord.[a]	Cat.-H_2O distance (Å)	nH_2O (per cation)	nH_2O shared (p.f.u.)
Mg-SWy	16.02 ±0.07	2.16	6.19 ±0.03	0.00	0.72/VI	4.28	13.72 ±0.40	0.14 ±0.04
Ca-SWy	15.34 ±0.05	2.52	7.93 ±0.06	0.00	1.12/VIII	4.87	15.68 ±0.45	0.30 ±0.05
Ba-SWy	15.19 ±0.06	2.79	9.34 ±0.12	0.00	1.42/VIII	4.92	15.12 ±0.44	0.40 ±0.06
Na-SWy	14.82 ±0.06	2.43	5.74 ±0.10	0.10 ±0.03	1.02/VI	4.73	14.93 ±0.34	2.22 ±0.14

Note: Inter-species distances and numbers of H_2O molecules are extracted from the radial distribution functions and hydration number functions, respectively, shown in Figure 5.

[a] From Shannon (1976)

Table 3. Structural parameters of the different planes of interlayer species approximating the atomic density functions derived from GCMC simulations.

	1st plane of H_2O molecules			2nd plane of H_2O molecules			Plane of interlayer cations		
Sample	*z*-position	quantity	B	*z*-position	quantity	B	*z*-position	quantity	B
Mg-SWy	± 3.61	3.23	12.6	± 1.29	4.84	104	0.00	0.1875	44.4
Ca-SWy	± 3.47	3.05	12.6	± 1.35	4.57	104	± 0.60	0.1875	38.7
Ba-SWy	± 3.44	3.14	12.6	± 1.27	4.46	104	± 0.85	0.1875	23.9
Na-SWy	± 3.37	3.15	12.6	± 1.20	4.25	104	± 1.20	0.3750	25.7

Note: The *z*-positions (in Å) of the different planes are given relative to the interlayer mid-plane. The quantity of interlayer H_2O molecules and cations are given per formula unit, whereas the Debye-Waller factor (B) is given in Å^2.

Table 4. Simplified interlayer structure model allowing XRD simulation of 3W smectite.

3-Water; d_{001}=18.5-19.2 Å		
z-position (Å)	Quantity (p.f.u.)	B (Å^2)
± 3.50(15)	3.15(15) H_2O	10-15
± 1.27(12)	4.50(45) H_2O	~100
± 0.00-1.20[a]	0.5 M^+	20-45

Note: The *z*-positions of the different planes are given relative to the interlayer mid-plane.

[a] The actual position of cation planes may be approximated from the linear regression equation shown on Figure 9.

FIGURE CAPTIONS

Figure 1. Simulation box for Grand Canonical Monte Carlo simulation of 3W Ca-SWy montmorillonite. The rigid box encompasses 6 × 4 unit cells along the *a* and *b* directions, respectively, and three interlayers. The layer-to-layer distance is constrained by experimental d_{001} values. During simulations, the clay box is equilibrated with a water vapor reservoir set at 98% RH. Water molecules can enter or exit the interlayer spaces and all interlayer species (H_2O molecules and cations) can move to reach an equilibrated state.

Figure 2: Interlayer configurations deduced from GCMC simulations. (a) Atomic density profiles of hydrogen (dotted line), oxygen (solid line), and cations (bold solid line). (b) Electron density profiles for H_2O (solid line) and cations (bold solid line). (c) Comparison between electron density profiles of interlayer H_2O from GCMC simulations (gray solid line) and the approximation by discrete planes of H_2O molecules (dotted line). The solid line sums up the contributions of the different planes for the latter model. (d) Comparison between electron density profiles of interlayer cations from GCMC simulations (gray solid line) and the approximation by discrete planes of cations (dotted line). The solid line sums up the contributions of the different planes for the latter model.

Figure 3. Experimental and calculated XRD patterns of 3W montmorillonite. Experimental patterns are shown as solid circles whereas calculated profiles generated from (a) GCMC simulations or (b) simplified interlayer models (see text for details) are shown as gray solid

lines. Vertical gray bars indicate the scaling up of the high-angle region intensities with respect to the 2-6° 2θ region. Difference plots are shown at the bottom of the figure and display reflections from accessory minerals.

Figure 4. Sensitivity tests of calculated XRD profiles to the interlayer configuration for Mg-SWy. (a) Influence of the interlayer H_2O content. The GCMC optimized H_2O content was varied by ± 10% (Table 2). (b) Influence of the z-coordinates of H_2O molecules. The distribution profile of interlayer H_2O shown in Figure 2a was stretched along the *z*-axis to shift the two discrete and sharp maxima at ~2.7 Å from the 2:1 layer by 0.1 Å. Arrows indicate significant misfits between experimental and calculated intensities. Others labels and notations as in Figure 3.

Figure 5. GCMC computed radial distribution function [$g_{\text{cat.-O}}(r)$ – solid line] and associated number of H_2O molecules around interlayer cations [$N(r)$ – gray solid line].

Figure 6. Atomic density profiles for the different type of interlayer H_2O molecules. (a) H_2O molecules from the first hydration shell are shown in black, whereas H_2O molecules filling the interlayer space appear in gray. (b) H_2O molecules from the first and second hydration shells are shown in black, H_2O molecules filling the interlayer space appear in gray. Oxygen, hydrogen, and cations are shown as solid, dotted and bold solid lines, respectively.

Figure 7. Snapshots of the GCMC computed configuration of H_2O molecules from the cation first hydration shell in 3W smectite. Each configuration is shown in projection along the *b*- and *c*-axes (top and bottom, respectively). H_2O molecules not from 1HS are shown as sticks to highlight cation first hydration shell polyhedra (in gray).

Figure 8. Snapshots of the GCMC computed configuration of H_2O molecules from the cation second hydration shell in 3W smectite. Projections and patterns as in Figure 7.

Figure 9. Distance from interlayer cation to the surface of the 2:1 layer in 3W smectite as a function of the cation ionic potential (valence over ionic radius ratio). Ionic radii considered are listed in Table 2.

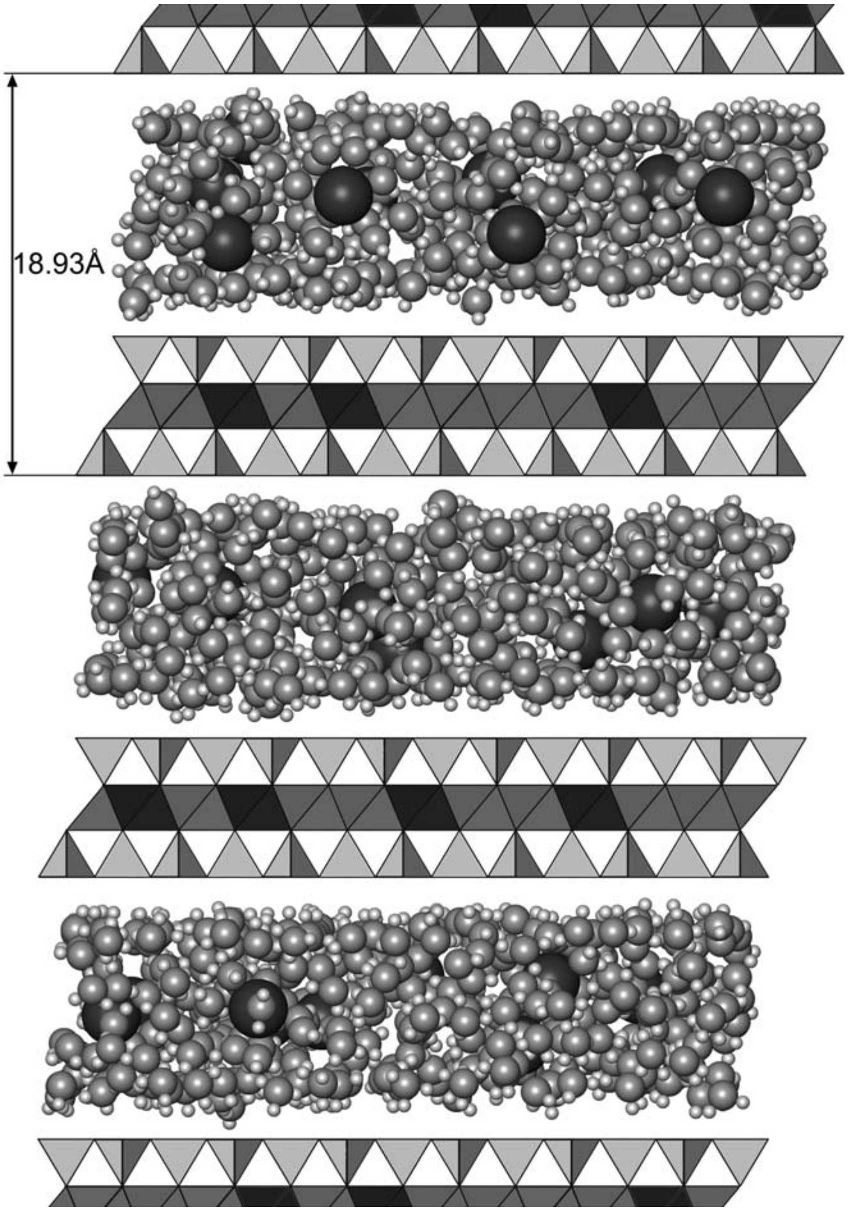
18.93Å

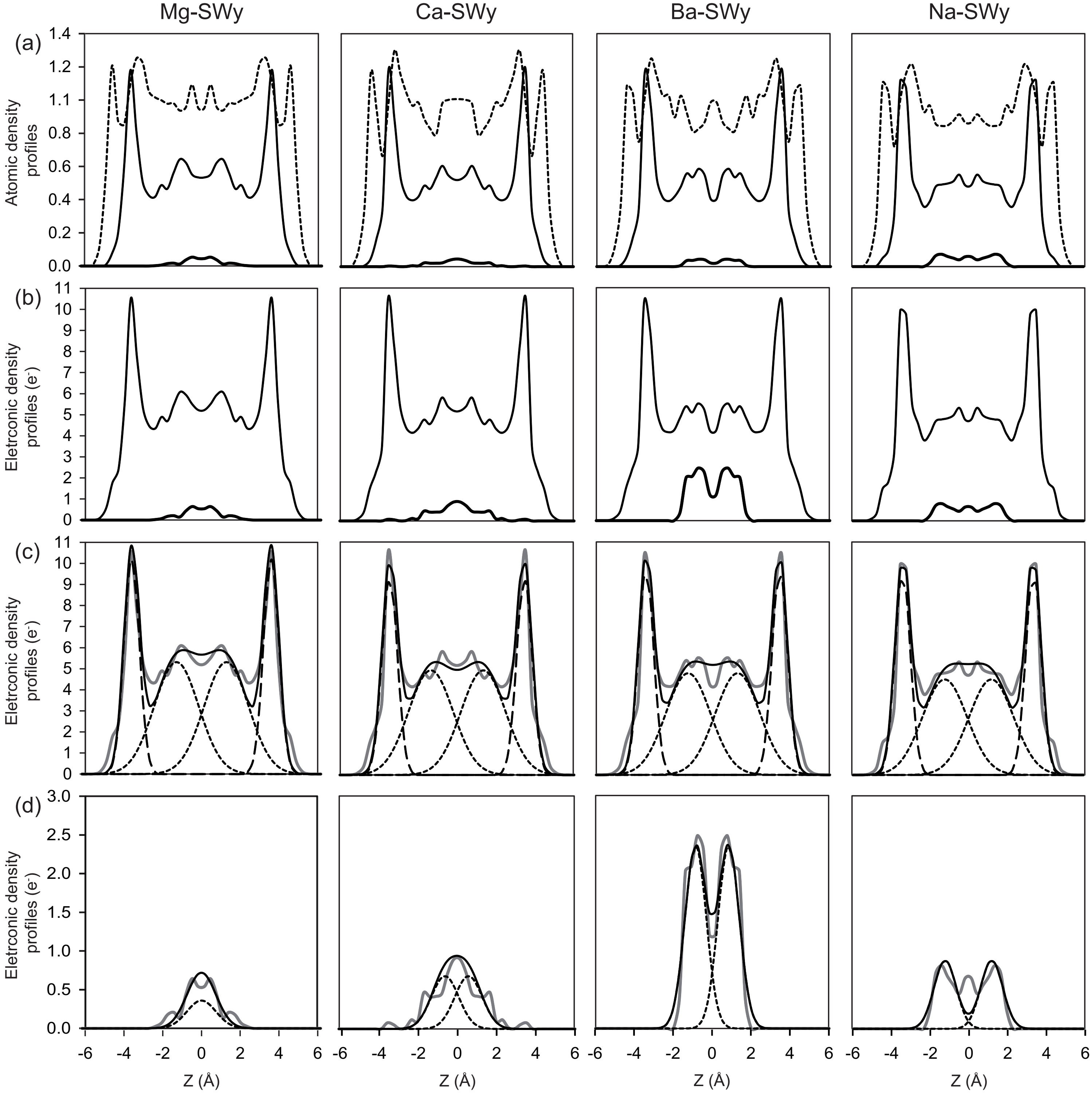
Mg-SWy
Ca-SWy
Ba-SWy
Na-SWy
(a)
(b)
(c)
(d)
Atomic density profiles
Eletrconic density profiles (e-)
Eletrconic density profiles (e-)
Eletronic density profiles (e-)
0.0
0.2
0.4
0.6
0.8
1.1
1.2
1.4
0
1
2
3
4
5
6
7
8
9
10
11
0.0
0.5
1.0
1.5
2.0
2.5
3.0
-6
-4
-2
0
2
4
6
Z (Å)

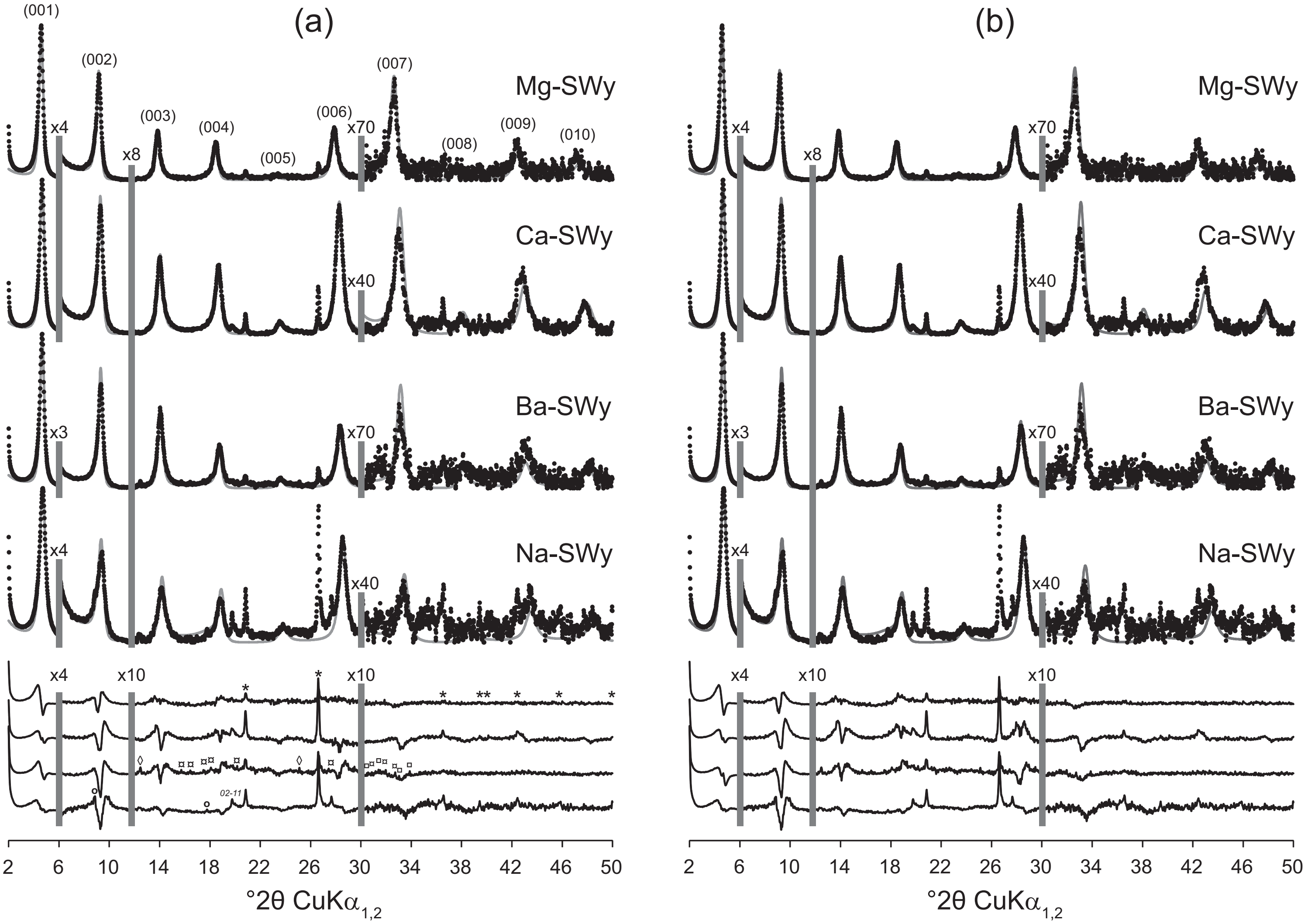
(a)
(b)
(001)
(002)
(003)
(004)
(005)
(006)
(007)
(008)
(009)
(010)
Mg-SWy
Ca-SWy
Ba-SWy
Na-SWy
x4
x8
x70
x40
x3
x70
x4
x40
x4
x10
x10
02-11
2 6 10 14 18 22 26 30 34 38 42 46 50
°2θ CuKα1,2

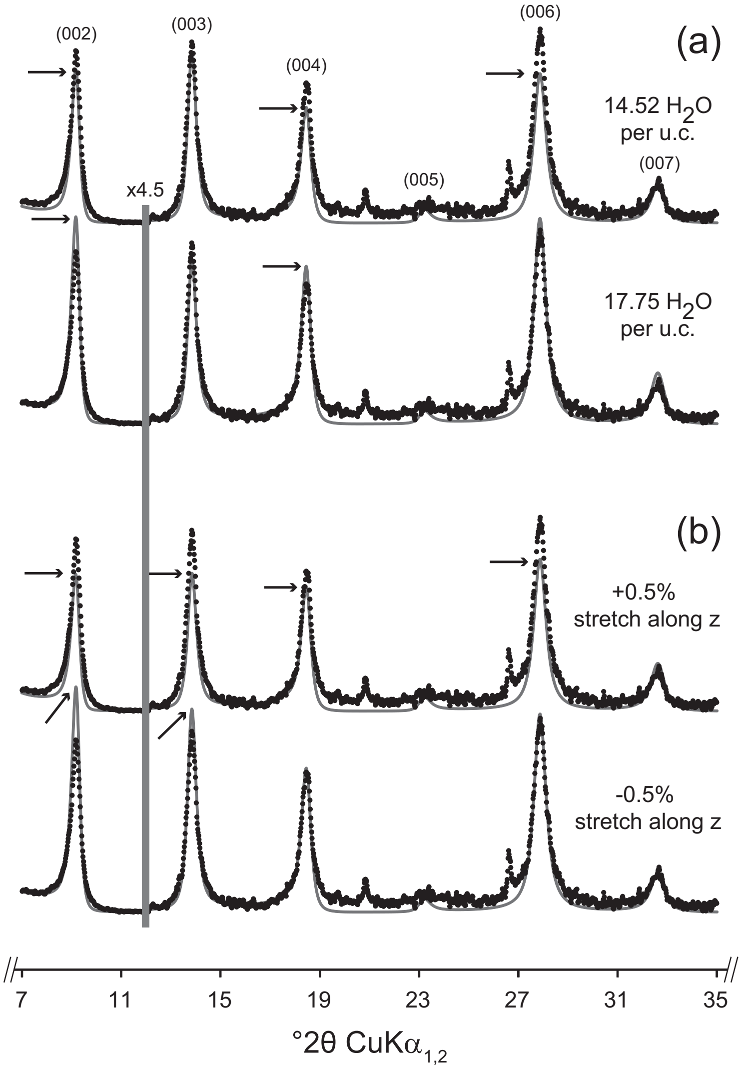
(002)
(003)
(004)
(006)
(005)
(007)
(a)
14.52 H_2O per u.c.
x4.5
17.75 H_2O per u.c.
(b)
+0.5% stretch along z
-0.5% stretch along z
7
11
15
19
23
27
31
35
°2θ CuKα$_{1,2}$

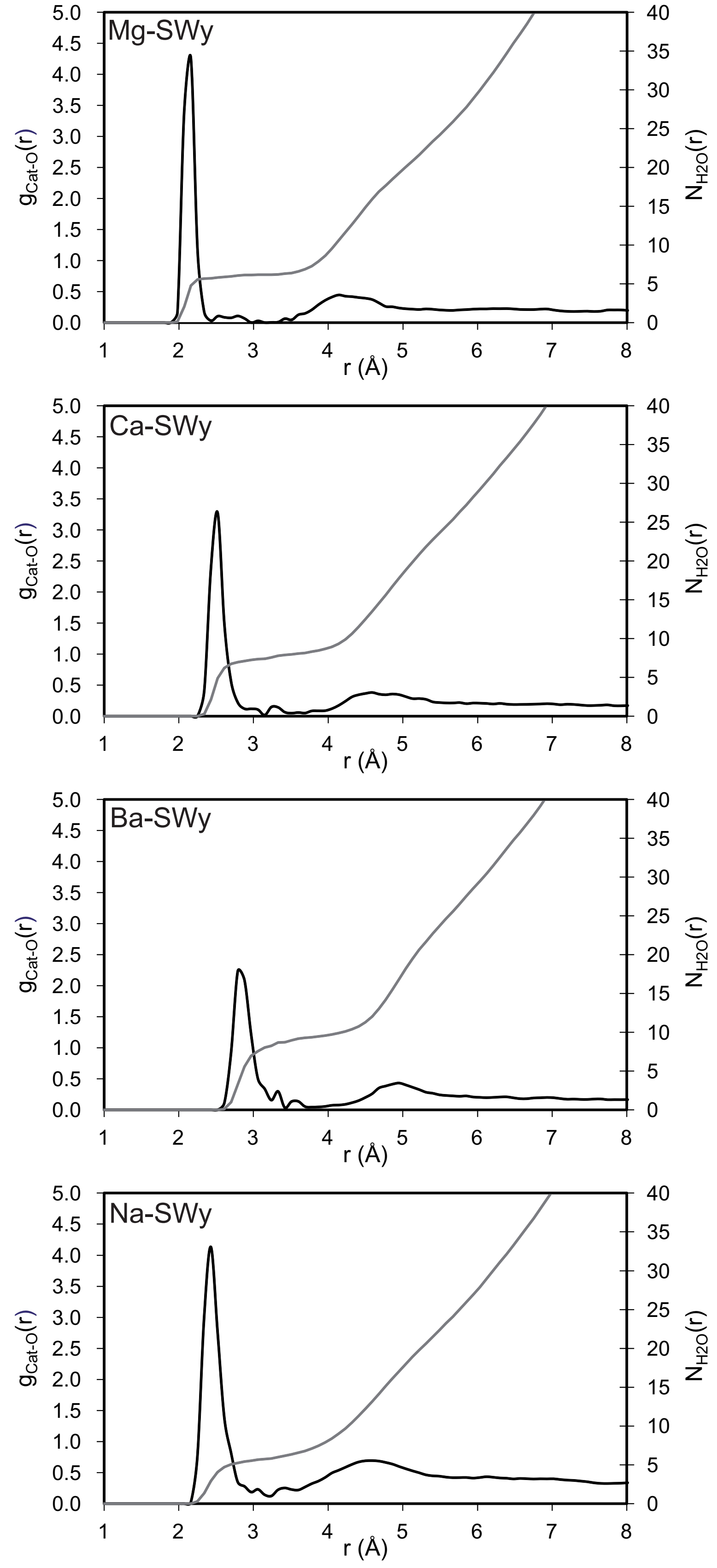
Mg-SWy
Ca-SWy
Ba-SWy
Na-SWy
$g_{Cat-O}(r)$
$N_{H2O}(r)$
r (Å)
0.0
0.5
1.0
1.5
2.0
2.5
3.0
3.5
4.0
4.5
5.0
0
5
10
15
20
25
30
35
40
1
2
3
4
5
6
7
8

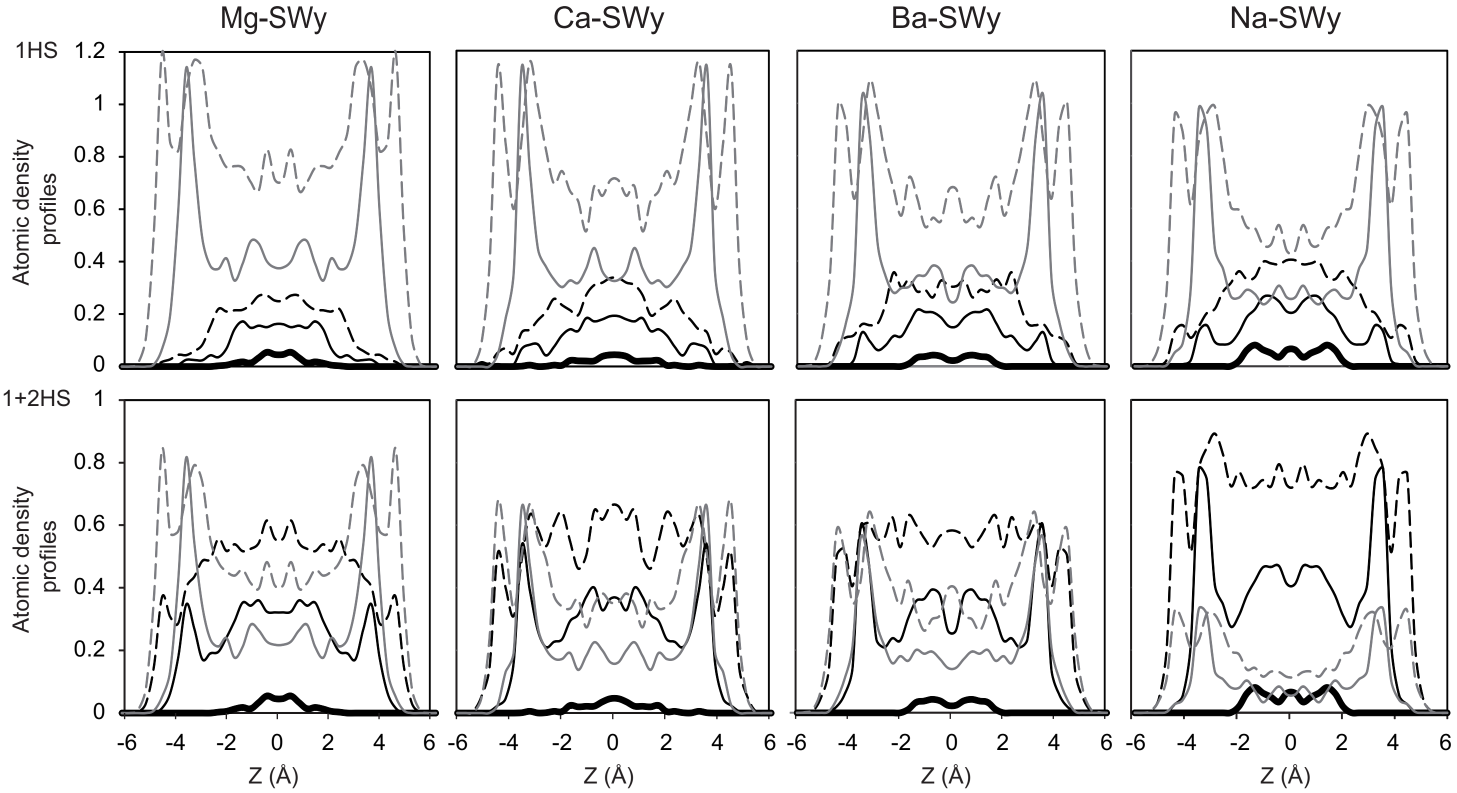
Mg-SWy
Ca-SWy
Ba-SWy
Na-SWy
1HS
1+2HS
Atomic density profiles
1.2
1
0.8
0.6
0.4
0.2
0
-6
-4
-2
0
2
4
6
Z (Å)

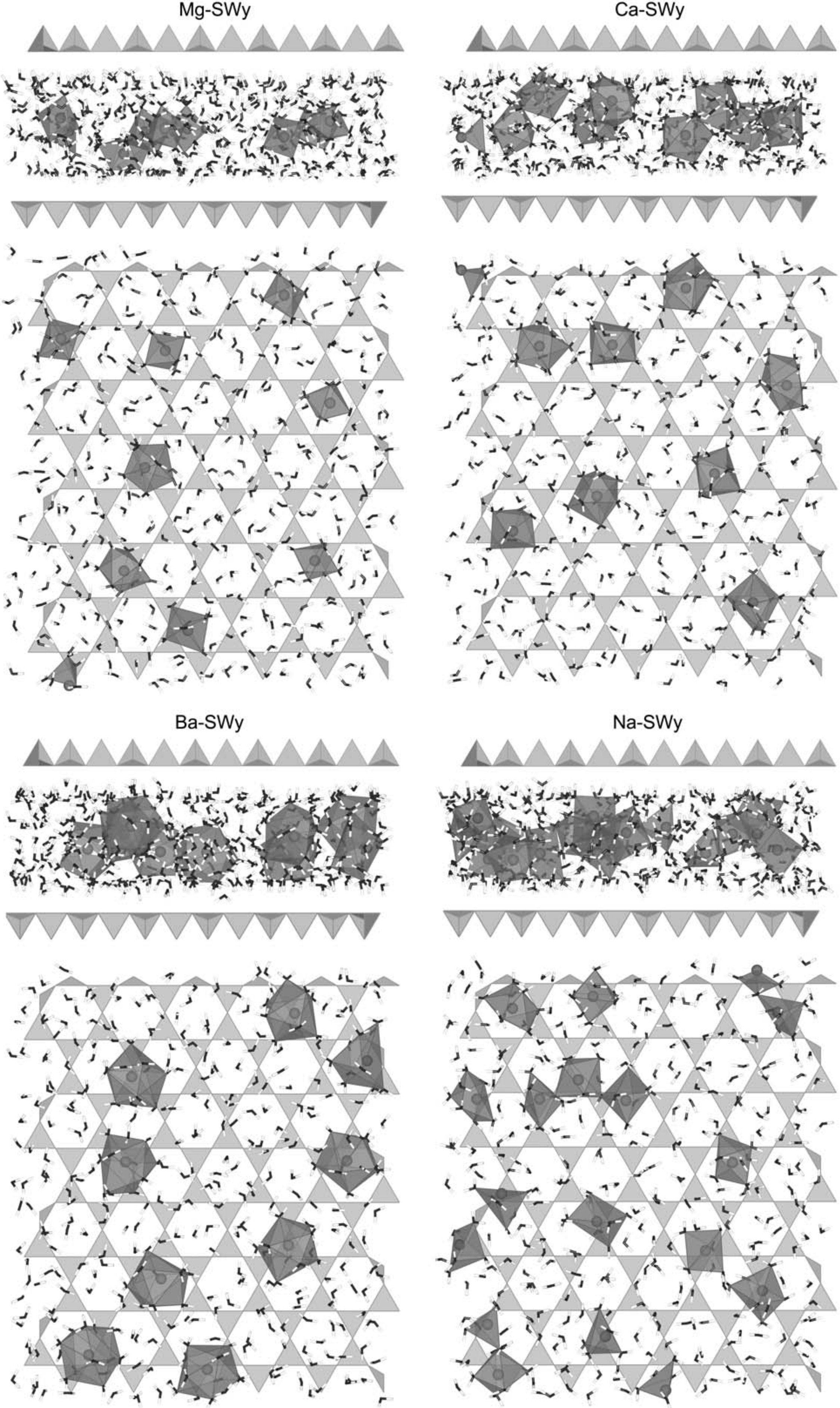
Mg-SWy
Ca-SWy
Ba-SWy
Na-SWy

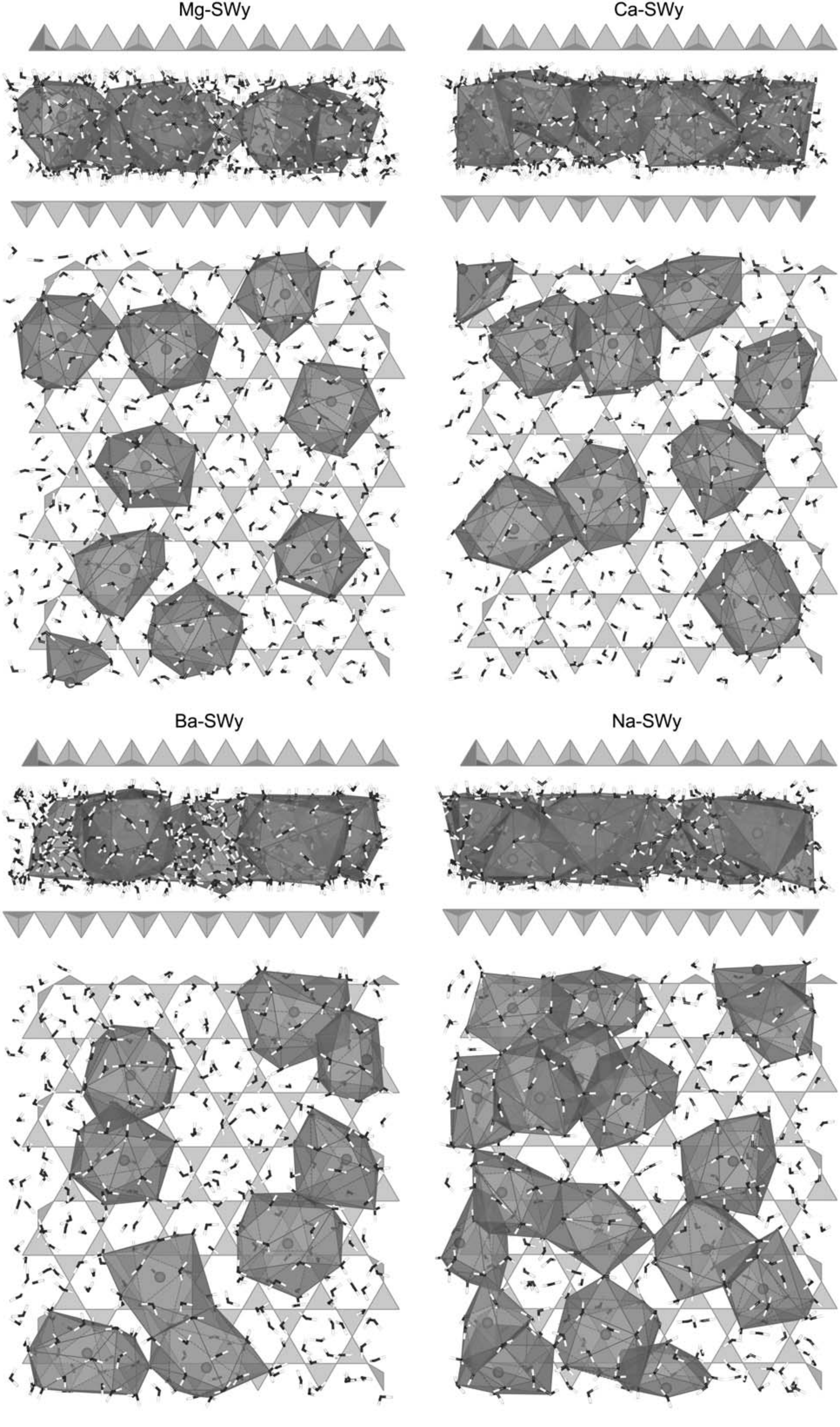

Mg-SWy

Ca-SWy

Ba-SWy

Na-SWy

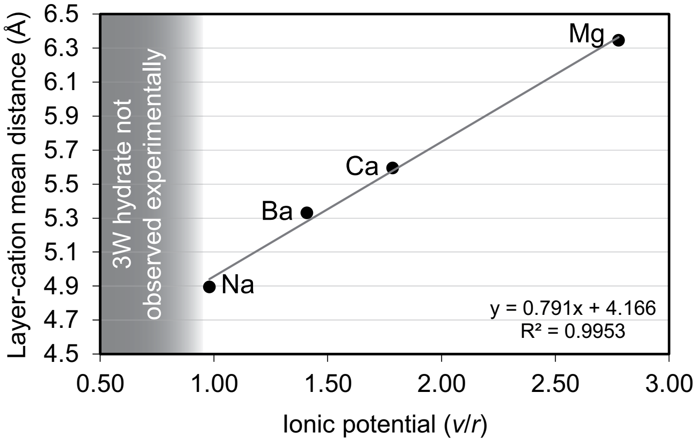
Layer-cation mean distance (Å)
6.5
6.3
6.1
5.9
5.7
5.5
5.3
5.1
4.9
4.7
4.5
3W hydrate not observed experimentally
Mg
Ca
Ba
Na
y = 0.791x + 4.166
R² = 0.9953
0.50
1.00
1.50
2.00
2.50
3.00
Ionic potential (v/r)